An investigation of a Heavy-fermion insulator and Quantum spin liquid candidate

by **Anish Parulekar**

March 21st 2024

Gang Cao, Thesis Advisor, Department of Physics

Paul Beale, Honors Council Representative, Department of Physics

Rishi Raj, Outside Reader , Department of Mechanical Engineering

A thesis submitted to the University of Colorado

in partial fulfillment of the requirements

for the designation of departmental honors

Department of Physics

Abstract

Heavy-fermion metals, strange metals, and quantum spin liquids all represent unique and exotic states of matter. They typically are present and discussed in distinct materials. To investigate a material that seems to have all three quantum states, a complete round of physical property measurements was conducted. This thesis represents a part of a larger investigation into:

$$Ba_4Nb_{1-x}Ru_{3+x}O_{12}(|x| < 0.20)$$

[[1]] This paper will be looking at the Heat capacity, resistivity, magnetization, composition, growth, and Hall effect data for this sample. This discussion will start with the theoretical explanation of all the terminology as well as the motivation for this study. Next, there will be a detailed explanation for the theory of operation for all of the data represented. Finally, the data will be represented and it's consequences analysed and discussed. One thing of note here is that the theoretical model will be a brief explanation on the different exotic states discussed rather than an overview for this specific material. It is important to remember here there is no agreed upon model that serves as an explanation of this exotic material.

Acknowledgements

I want to thank everyone who has played a key role in my growth as a physicist. Specifically, I want acknowledge Yu Zhang, Yifei Ni, and Hengdi Zhao for inspiring me to pursue further degrees and their infinite patience in answering all my questions. I want to particularly thank Professor Gang Cao who has been an amazing mentor over the past three years and has been integral to my interest in research. Lastly, I thank my parents who have supported me throughout my life and inspired my journey into physics.

Contents

List of Figures

1 Introduction

1.1 Motivation

Synthesizing and characterising exotic materials play a key role in discovering new and exotic physics in quantum materials. Trimmer systems in particular have been a recent avenue for our group to discover novel materials. They have been proved to have a variety of quantum states. One of these quantum states, quantum spin liquids, have a possible application in quantum computing, specifically topological quantum computation. If these particle excitations can be isolated, they could be implemented in topological quantum computation. These topological quantum computers would be much more stable when compared to traditional trap based quantum computers. Investigating novel superconductors using well understood doped quantum spin liquids is another avenue of application with large ramifications. Superconductors would revolutionize energy grids and energy usage. Grids and electrical lines would have essentially zero waste, drastically reducing the amount of energy lost to resistance and hence, heat. Almost 6 percent of all energy generated is lost in transmission. Major reduction of loss in power generation up to 40 percent could significantly decrease the amount of energy required. There are also possible avenues in energy storage as a loop of superconductors could run current for months serving as a form of battery without any loss in electrical energy. The efficiency gains from superconductors can not be understated and will serve a key role in the current energy crisis the world is in.

1.2 Overview

In this thesis I will start by giving a theoretical background of the three quantum states that will be discussed. The states that will be discussed are quantum spin liquids, strange metals, and heavy-fermion metals. I will then be discussing the material:

$$Ba_4Nb_{1-x}Ru_{3+x}O_{12}(|x| < 0.20)$$

and the theoretical background into what could be driving the interesting behavior seen. I will then be delving into the methods section where I will start with the Physics Property Measurement System (PPMS) and how the hall effect, heat capacity and resistivity data was collected. In particular I will briefly discuss the theory of operation for each measurement as well as sample preparation. This alongside the magnetization measurements using a SQUID paint the picture of the multiple exotic states seen in this material. I will end the methods section with how the sample was grown as I have been able to successfully grow these samples to have a complete thesis. However, the data shown are on samples grown by my PI. I will then be showing and explaining the data we have collected and how it can be understood to identify these quantum states. While my work has focused on the insulating state of this material, I will be explaining the metallic phase as well. I will also be citing the Arxive paper for the metallic data.

2 Theory and Background

2.1 Introducing $Ba_4Nb_{1-x}Ru_{3+x}O_{12}(|x| < 0.20)$

[[1]] The material discussed in this paper has a rhombohedral structure with space group R-3. The trimers which consist of 3 face sharing octahedra play a key role in the interesting physics discussed later as our group has investigated multiple trimer systems that have produced exotic states. The material's quantum states depends on the amount of Niobium doped into the sample; at the lowest amount the sample displays a heavy-fermion strange metal. At the highest amount an insulating phase discussed in detail here. The phase diagram shown below serves as an useful depiction of this change in states, however, there is a lot of detail in this diagram that will be explained later in this thesis.

Figure 1: Structure of $Ba_4Nb_{1-x}Ru_{3+x}O_{12}(|x| < 0.20)$ [[1]]

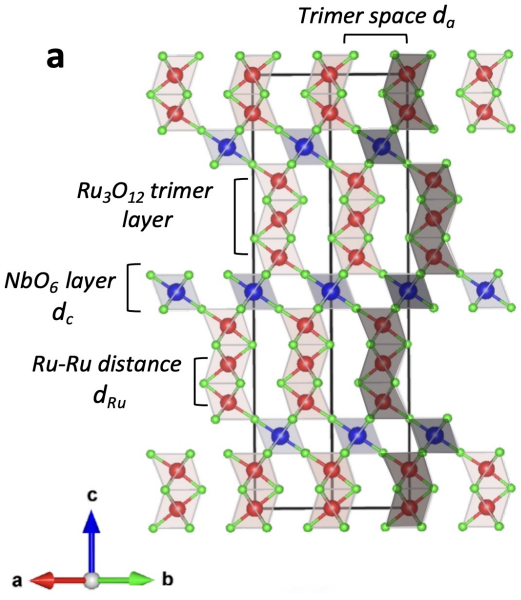

Figure 2: States of $Ba_4Nb_{1-x}Ru_{3+x}O_{12}(|x| < 0.20)$ [[1]]

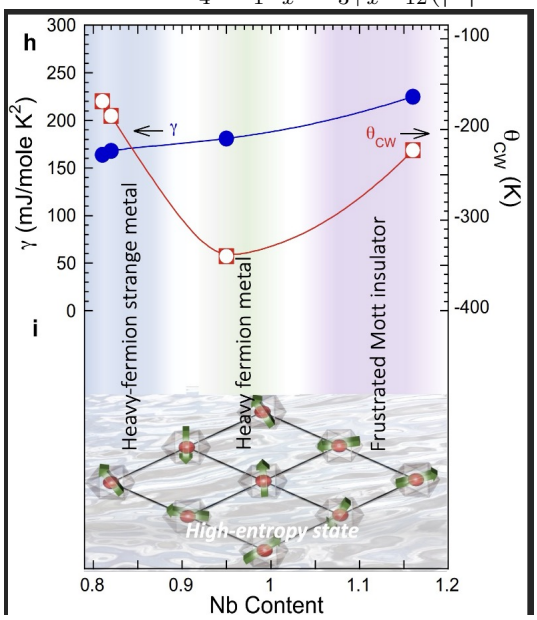

2.2 Heavy-fermion behavior and the Fermi surface

[[2]]The most logical place to start the discussion of the exotic quantum states is in heavy-fermion metals. This is because this behavior is predicted by the well established Fermi liquid theory. The name heavy-fermion clues us into its defining property of the γ factor being larger than expected from the mass of these electrons. γ represents the electronic contribution to heat capacity. This behavior is typically driven by f-electrons with strong electron-electron interactions. In these heavy-fermion materials the interaction is between the localised f-electrons and the itinerant conducting electrons.

The Kondo effect is crucial to understanding these interactions. It describes the interaction between localised magnetic moments from the f-electrons and the itinerant conducting electrons. [[3]] For local magnetic moments to arise the Coulomb

interaction must get rid of all high energy fluctuations leaving only low energy spin states. The combination of spin and orbital angular momentum can be described using:

$$\vec{j} = \vec{l} + \vec{s}$$

With $\vec{l}$ being the angular momentum from the orbital and $\vec{s}$ being spin.

The main point to focus on is the creation of a Kondo singlet via the strong coupling between the electrons in the conduction sea and the localized magnetic moments. This singlet can be represented by:

Figure 3: Kondo Singlet [[3]]

$$|GS\rangle = \frac{1}{\sqrt{2}}(|\Uparrow\downarrow\rangle - |\Downarrow\uparrow\rangle),$$

The double arrow represents the local magnetic moment and the spin from the conducting electron is represented by the single arrow. If a lattice is full of local magnetic moments, there can be coherence between these Kondo singlets forming a Kondo lattice. Now due to this following Fermi liquid theory we expect to see resistivity to follow $\rho = \rho_0 + cT^2$. The Fermi sea gets created around the singlet above. However, as we will see later, it is important to discuss non-Fermi heavy-fermion behavior. There are a few characteristics which are common and expected from heavy-fermion materials. These include the large γ factor that causes a linear heat capacity in low temperatures, the relationship between temperature and resistivity discussed above, and lastly the high temperature magnetization should follow Curie-Weiss. For more details, see the methods section on magnetization.

Kondo insulators have been discovered and investigated. One example would be $Ce_3Bi_4Pt_3$[[4]], where the Ce moment causes an insulating gap to occur. Kondo insulators act metallic at high temperatures, but at lower T, Kondo singlets form that screen the dense magnetic moments resulting in a gap. The last Kondo lattice I will mention is LiV_2O_4 where it's generally agreed on that magnetic frustration is the root cause of this heavy-fermion metal[[5]]. Frustration plays a key role in potentially explaining the heavy-fermion behavior we investigate later.

Figure 4: Kondo coupling [[3]]

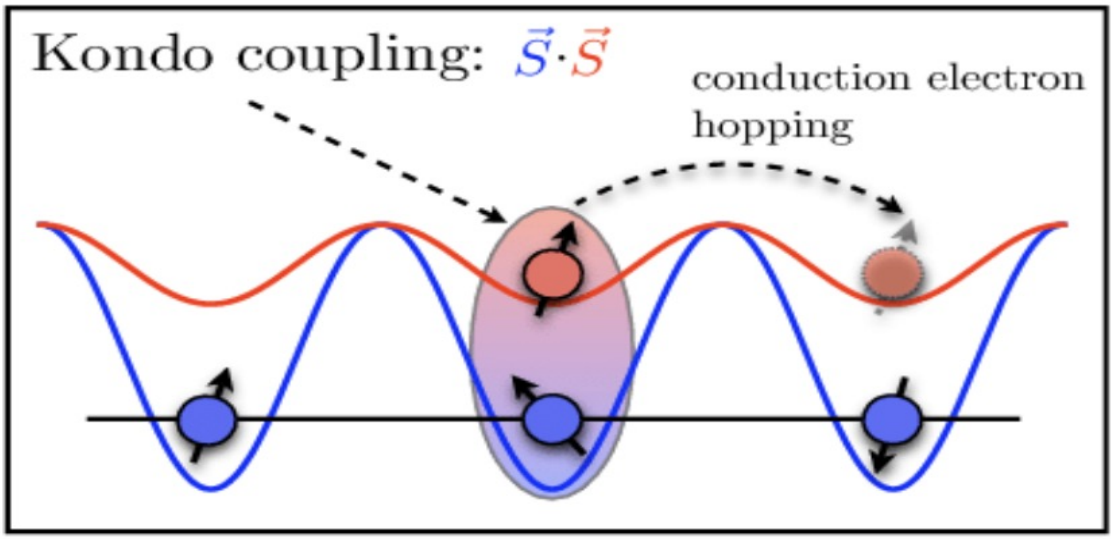

2.3 Strange metals

Strange metals are important to understand the metallic phase of the material, however, I will not spend long discussing this as my work focuses on the insulating state. Strange metals are defined by their linear dependence of resistivity against temperature. This is in sharp contrast to the T^2 relationship described by the widely successful Fermi liquid theory.[[6]] This is mainly driven by the scattering rate of the charge carries at the Planckian limit, or in essence $\rho(T) \propto$ T. One thing to note here, is that strange metals fall outside the purview of Fermi liquid theory, this is in contrast to heavy-fermion metals whose typical explanation can be found inside Fermi liquid theory.

2.4 Quantum spin liquids

The last exotic state to discuss are quantum spin liquids. [[7]] QSLs defining characteristic is the lack of long range magnetic order. This lack of order is driven by long range entanglement between spins. This definition of QSLs is not universally agreed on, nor are its mechanisms. Instead discussing why a lack of order is unusual at low temperatures is more useful. As the temperature is lowered, entropy is removed from the system, this removal in most materials leads to ordering between the spins of the system, leading to a long range magnetic order such as ferromagnetic or antiferromagnetic states. The idea of long range entanglement is in essence where the entanglement between multiple spins doesn't allow this to occur. One spin-1/2 is entangled to two others in an anti-parallel arrangement. QSLs are also thought to be Mott insulators. While most of the literature has focused on honeycomb lattices, research into triangular lattices has predicted linear heat capacity against tempera-

ture boasting a large γ factor discussed above. Other than looking at magnetization data, a material that has magnetic orders at low temperatures can have a λ peak in the specific heat vs temperature [[8]]. QSLs do not have such a peak present. Ideally to properly identify QSLs, magnetization at zero temperature should be measured, due to practical limitations low temperature data can be used to extrapolate this.

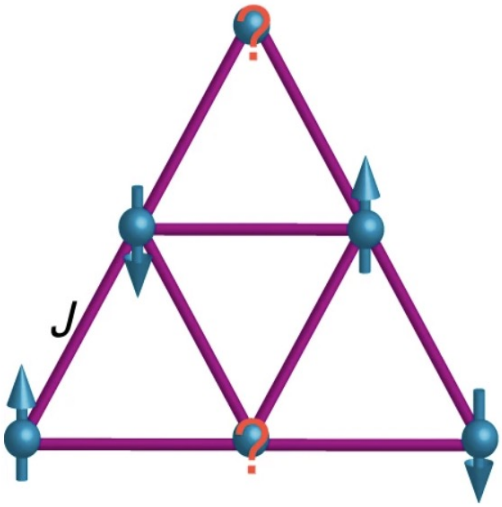

Figure 5: Triangular lattice QSL [[8]]

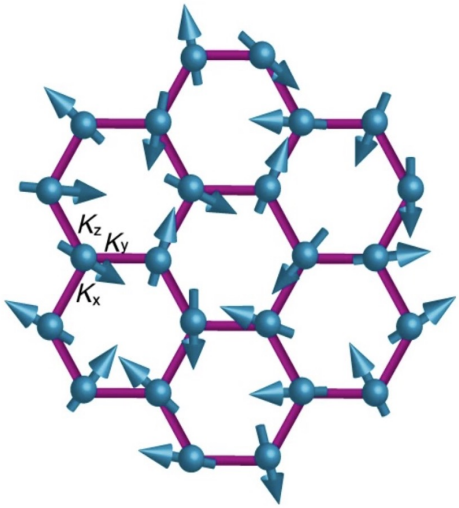

Figure 6: Honeycomb lattice QSL [[8]]

J represents the Heisenberg exchange interaction.

3 Research Methods

3.1 Physical Property Measurement System

Temperature control and external magnetic field operation have the same theory of operation in the Quantum Design 14T-PPMS-Dynacool system (PPMS) regardless of measurement type. Temperature control in the PPMS is full of precise insulation against convection, conduction and radiation. A full explanation of specifics would be unnecessary and so I will be focusing on the overview of this precise temperature control.

High Temperature control is managed by a series of heaters and cold helium vapor. A heater is used at the bottom of the sample chamber while a heater at the top of this chamber reduces thermal gradients. The sample itself sits on a puck near the block heater that will be discussed later. Below 4.2 K a mixture of liquid helium and helium vapor is used to cool the sample chamber to 1.8 K.

Magnetic fields are controlled using superconducting electromagnets whose current is precisely controlled while being in a liquid helium bath to keep the temperatures below the critical T. These magnets allow us to take measurements in a -14 T to 14 T external magnetic field.

3.1.1 AC Resistivity and IV [ETO]

Resistivity plays a key role in determining some of the most basic characteristics of a material such as it being an insulator or metal. AC electrical resistivity and IV measurements were taken using the standard four-leads method where the I+ and I- leads are on the edges of the sample while the V+ and V- leads are placed

in between. The four-leads method prevents contact resistance from affecting the measured values. The leads are made out of 0.0025-mm diameter gold wire and is attached to the sample using H20E silver epoxy. Both of these are generally more conducting when compared to the samples studied and hence reduce contact and wire resistance. A representation of the electrical transport puck used can be seen below. 3 total samples can be mounted on to the puck while 2 samples can be measured at the same time. The 4-lead method can also be seen with where the leads attached are labelled.

Figure 7: Electrical transport puck [[9]

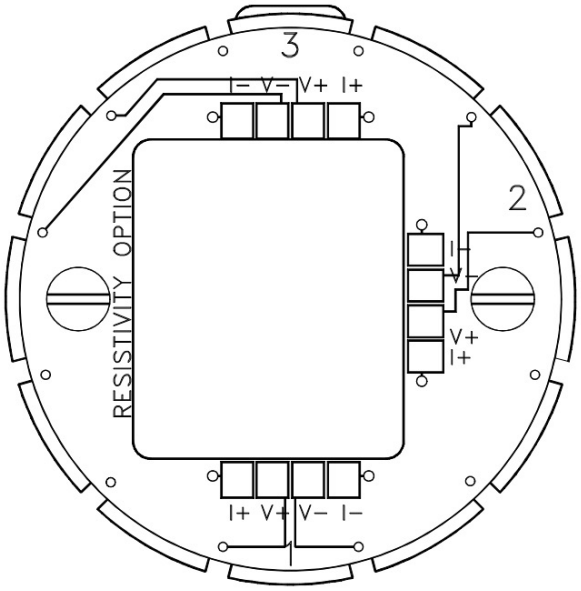

3.1.2 Heat capacity

Heat capacity is a significant measurement that indicates the kind of phase transition being studied. For example a lambda-peak indicates a 2^{nd}-order transition

whereas a discontinues curve could indicate a 1st-order transition.

For this thesis low temperature heat capacity is significant as it tells us the phonon and electronic contribution to heat capacity. The contribution from phonons at low temperatures can be described using the Debye T^3 relationship [[10]]:

$$C_p = \frac{12\pi^4 N_A k_B}{(5T_D^3)T^3} = \beta T^3$$

where N_A represents Avogadro constant, k_B is the Boltzmann constant, and T_D is Debye temperature.

The electronic contribution to heat capacity is linear in nature. The electrons contributing to this are assumed to be near the Fermi level in terms of energy. The linear coefficient γ is also called the Sommerfeld coefficient:

$$C_e = \gamma T$$

So the total value can be fitted to:

$$C_T = \gamma T + \beta T^3$$

The heat capacity measurements in this thesis were conducted in the PPMS. A clear representation of the puck used can be seen below found in the user manual [[11]]:

Figure 8: Heat capacity Puck [[11]

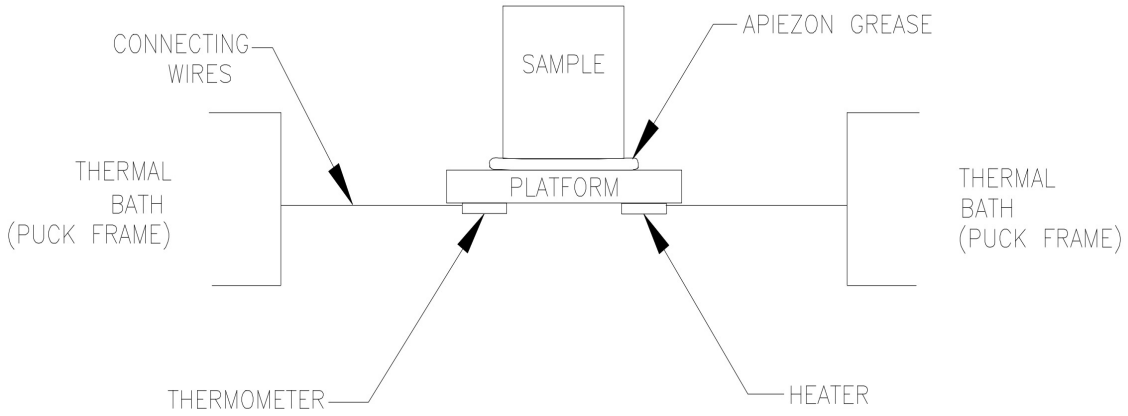

One small correction is that the grease that is applied typically covers the entire sample to better ensure consistent temperatures throughout the material. Here the puck itself acts as a thermal bath providing an avenue for excess heat to exit. The puck has a separate heater and Cernox thermometer to measure how much heat a sample can hold under a specific temperature and magnetic field. To prevent heat loss to the rest of the chamber via convection and conduction with gas, the chamber is placed under a ultra-high vacuum. To conduct a successful measurement there is a lot of calibration that must first take place. However, I will focus on the addenda measurement conducted prior to the sample measurement. This addenda provides a difference between just the sample holder's response and the sample holder plus the sample's response. The thermal grease is applied before the addenda to get an accurate measurement of just the sample not including the sample holder and thermal grease. This grease itself is only appropriate for temperatures below 200 K and this will be reflected in the data. The measurement starts by increasing the temperature by around 2 %. This heat is then dissipated through the palladium wires seen in the

diagram. The temperature vs time curve is then fitted to a model with:

$$\frac{dT}{dt}C_{total} = P - \kappa_w(T_s - T_O)$$

P represents the power function of the heater, κ_w is the known thermal conductivity of the wires and sample holder. T_s and T_O are the sample and starting temperatures respectively.

3.1.3 Hall effect

The Hall effect data is taken using the same electrical transport puck above. There are I+ and I- leads placed in one direction whereas the V+ and V- leads are then placed transverse to measure the transverse voltage difference across the sample. It is important to note here that due to limitations in the sample size and shape, the Hall effect data can be noisy but sufficient when establishing a general trend.

3.2 Magnetization

The magnetization data was taken on a Quantum Design MPMS-XL magnetometer (MPMS). The MPMS uses a SQUID to get precise magnetization data. The basics of the theory of operation is multiple loops running a controlled current. The sample oscillates through these loops while an external magnetic field is applied. The change in magnetic flux through these loops is converted to a change in the current signal and plotted against position of the oscillating sample after the center has been preset. This gives us the magnetization of the sample. The sample itself is mounted to a quartz rod using GE Varnish (VGE-7031). A SQUID is a superconducting quan-

tum interference device. A total of four coils are uses, two wound clockwise and two wound counterclockwise to cancel the signal from the external magnetic field applied in the MPMS. The driving principle behind the SQUID are two parallel Josephson junctions. These Josephson junctions are made out of two superconductors separated by an insulator. Cooper pairs can tunnel through this junction. In essence this measures the voltage created by the change in flux caused by the magnetization signal from the sample. The MPMS has a similar superconducting setup to the PPMS that can create up to a 7 T external magnetic field while varying the temperature between 300 K-1.8 K.

Multiple types of magnetic couplings can be seen using this method such as ferromagnetic, ferrimagnetic, and antiferromagnetic. Above the transition temperature the magnetization data can be used to establish the type of coupling present in the material. In this high temperature paramagnetic state the coupling can be described using Curie-Weiss law:

$$\chi = \frac{C}{T - \theta_{CW}}$$

C here is the Curie constant with units emu*K/mol[[12]]. θ_{CW} represents the Curie–Weiss temperature. Positive θ_{CW} represents a ferromagnetic coupling. Negative θ_{CW} represents an antiferromagnetic coupling, this however does not hold for frustrated systems as in these frustrated magnets one can usually still see a negative θ_{CW} but other interactions like entanglement do not allow an overall antiferromagnetic order to take place. θ_{CW} represents the molecular field within the material, hence the positive/negative correlation explained above. These frustrated states include quantum spin liquids discussed above. Magnetization also can show non-magnetic transitions such as charge density waves. Using the Curie constant we can calculate the effective

moment per ion in Bohr magnetons using $\sqrt{8C}\mu_B$. While focusing on Curie-Weiss paramagnetism, which involves an external field affecting the electron's angular momentum ground state, there are higher energy partially filled orbitals whose angular momentum does have an effect on the overall paramagnetic state. However, in most materials this contribution can be ignored.

Figure 9: Quartz rod with attached sample

3.3 Energy Dispersive X-ray Spectroscopy (EDX)

To characterize and identify the composition of the sample an EDX machine using the emission spectrum of the sample's surface is used. A representation of this can be seen below [[13]]. An incoming electron beam knocks off a bound orbital electron. This vacancy is then filled by an electron from a higher energy outer shell, when this electron falls in energy, it emits an photon in the X-ray range. The energy of this photon is unique to each element and is measured and compared to an established database. A Hitachi TM3030Plus was used for these EDX measurements.

Figure 10: Energy Dispersive X-ray Spectroscopy[[13]]

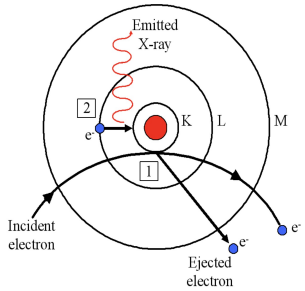

Figure 11: EDX example when calibrating

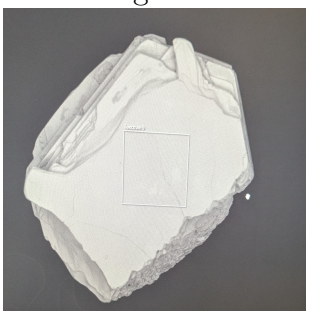

3.4 Sample synthesis

The sample was grown using a flux method. The exact details listed in this section only apply to the samples I have grown and not the samples from which the data was collected, however the general principle of flux growth remains the same. Flux method remains a common method of single crystal sample growth due to its simplicity and lack of complicated machinery. The flux acts as a solvent into which the components of the material desired dissolve into. There is a supersaturation that takes place as the temperature of the flux increases. The solutes are measured to be stoichiometrically correct. The solution then has nucleation points that act as the starting point for crystal growth, and as the temperature is lowered the supersaturation allows the single crystals to come out of the flux. While easy, the main drawback in using the Flux method is a lack of control of the nucleation points, this can lead to a wide variety of sample sizes and quality. This method starts with grinding the flux and solutes together until it visually resembles a homogeneous powder. This is then placed into a stable crucible typically made out of aluminum oxide or alumina. Then a sequence

with specific temperatures and heating/cooling rates is selected in a furnace. Lastly, the crystals are cleaned to remove any remaining flux, the EDX and XRD are used to identify the crystals. For the material discussed in this paper, $BaCl_2$ was used as the flux. $BaCO_3$, Nb_2O_5, and RuO_2 were the stable solutes for growth.

Figure 12: Alumina crucible used for flux growth

4 Results and Data

My main focus will be on $Ba_4Nb_{1.255}Ru_{2.745}O_{12}$ and $Ba_4Nb_{1.163}Ru_{2.837}O_{12}$. Looking at the phase diagram earlier we can see that given the high Niobium levels both of these materials are in the insulating state.

4.1 Resistivity for $Ba_4Nb_{1.255}Ru_{2.745}O_{12}$

Figure 13: Resistivity in ab direction

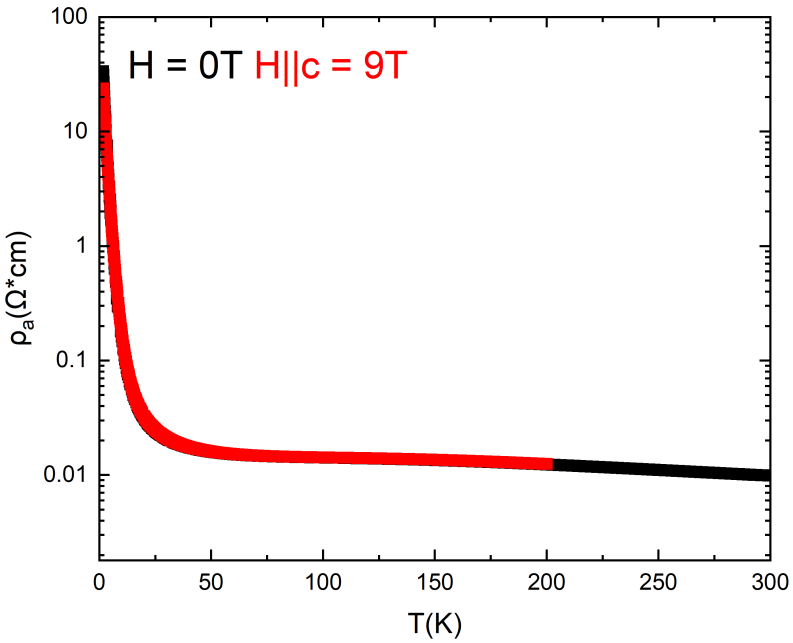

In the figure above, the field has been applied in the c direction corresponding to the same c-direction seen in the structure of the material (long direction). The behavior seen is a classic insulator, as the temperature decreases the resistivity of the sample increases almost exponentially (the scale is logarithmic), and slowly decreases at high T. The red indicates the resistivity of the sample when under a magnetic field of 9 Tesla. Since there is no significant deviation between the 0 and 9 Tesla data, the magneto-resistance can be considered insignificant. The insulating behavior indicates that the charge carriers/ electrons lose their thermal entropy, get localised and cannot carry current well through the sample. This is important to remember when analysing

the heat capacity data later. As the Niobium level of this sample is in between the two extremes the actual values of resistivity are not very high, but its insulating behavior can be identified using the trend.

Figure 14: Resistivity in c direction

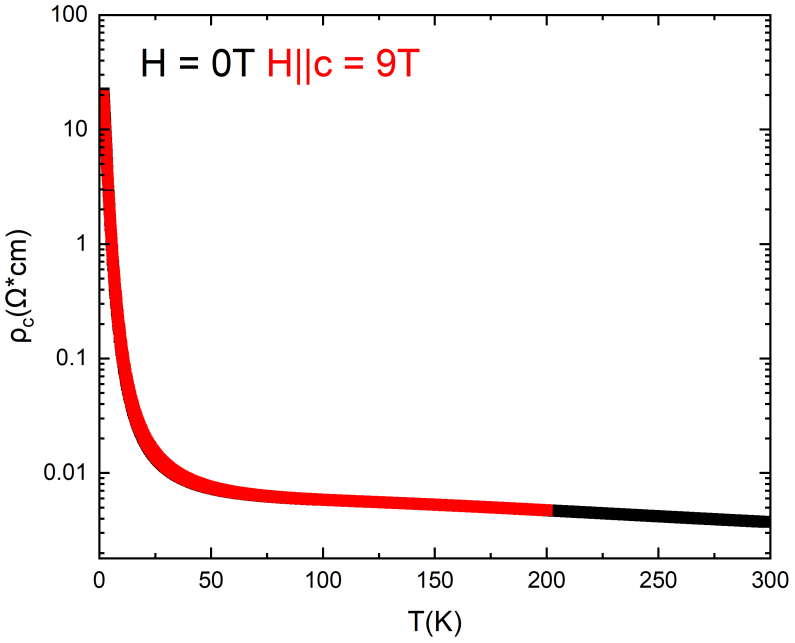

The same behavior is seen in the c-direction for resistivity, so no major anisotropy.

Figure 15: Field-sweep$_{ab}$

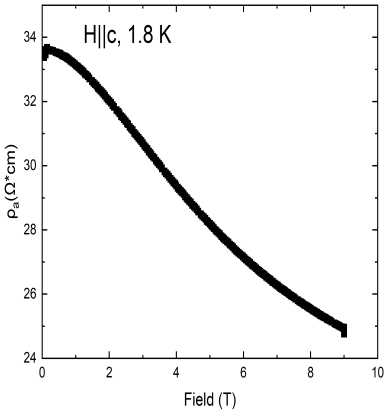

Figure 16: Field-sweep$_c$

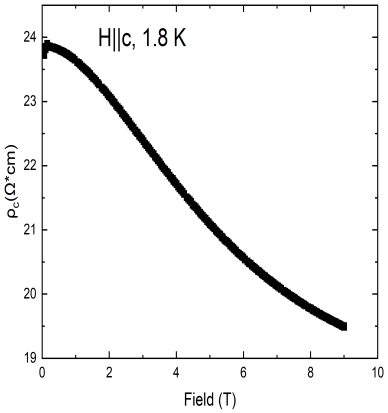

To see the lack of significant magneto-resistance better, above is a field-sweep, where the temperature is kept at 1.8 K and the field is swept between 0-9 Tesla. The drop in resistivity is relatively small, staying in the same order of magnitude. This indicates a small negative magneto-resistance.

4.2 Heat capacity for $Ba_4Nb_{1.255}Ru_{2.745}O_{12}$

To identify the heavy-fermion behavior for this material, taking a look at the heat capacity data is crucial.

To understand how this value for γ was calculated, starting with:

$$C_T = \gamma T + \beta T^3$$

Dividing by T:

$$\frac{C_T}{T} = \gamma + \beta T^2$$

If we then plot the $\frac{C_T}{T}$ against T^2 we can do a simple linear fitting where the intercept represents γ and the slope represents β.

Figure 17: Heat Capacity

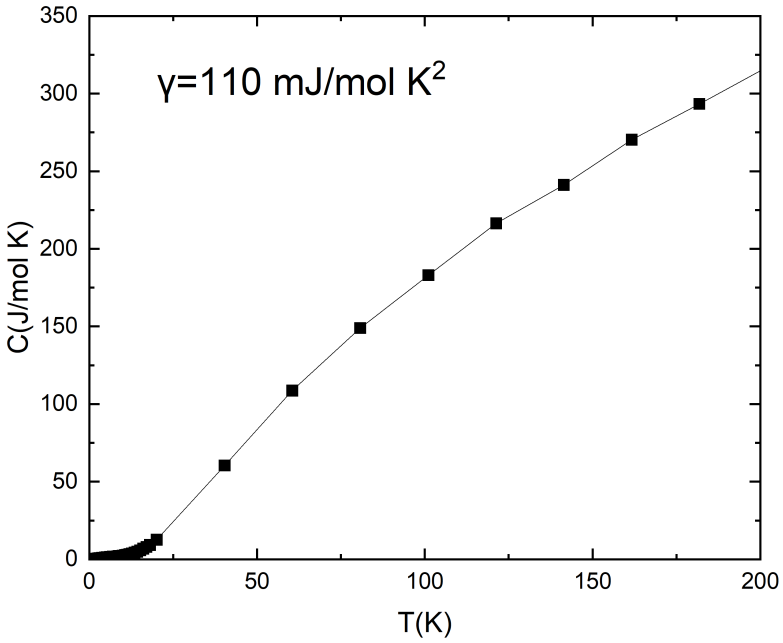

We can see that there is a distinct lack of a lack of a *lamda* peak indicating no low temperature magnetic order which will be discussed later. The γ coefficient is quite high at 110 $mJ/molK^2$. Anything above higher than 20 $mJ/molK^2$ is considered high enough for a material to be considered to be a heavy-fermion material.

Figure 18: Heat capacity fitting

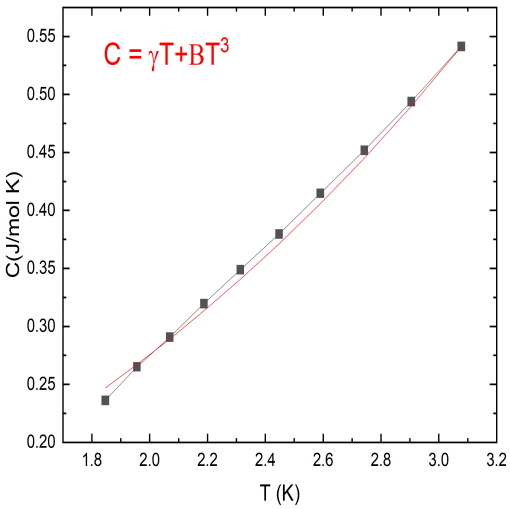

Figure 19: Heat capacity

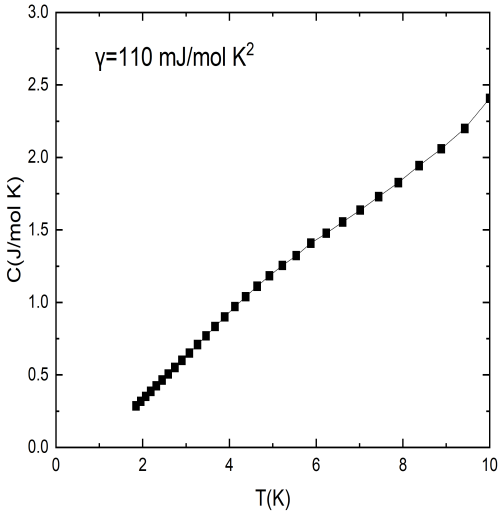

A better sense of how well the fitting works is demonstrated by **(Fig.18)**. It can be seen here that at very low temperatures the fitting (red) follows the general trend in the data (black). This strong linear behavior is also seen in a slightly longer temperature range in **(Fig.19)**. This is also interesting given that the sample is a typical insulator, so this raises the question if is in fact the electrons that are carrying heat since they get worse at carrying charge at lower temperatures. Regardless, the heavy-fermion state is confirmed with the data above.

4.3 Magnetization for $Ba_4Nb_{1.255}Ru_{2.745}O_{12}$

Plotting the magnetization along both ab and c-direction, we see that that as the temperature lowers, the material stays paramagnetic throughout. The increase in signal is due to loss in thermal entropy and the spins align themselves along the direction of the external magnetic field. A ferromagnetic transition would appear as

Figure 20: Magnetization$_c$

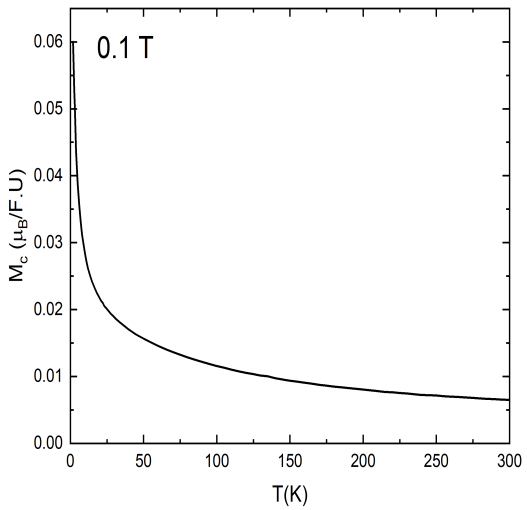

Figure 21: Magnetization$_{ab}$

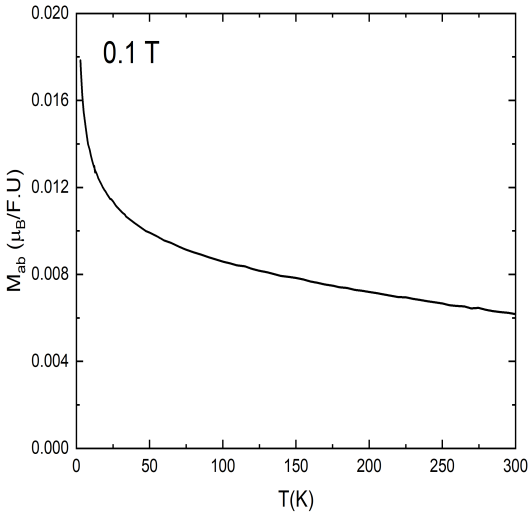

a significant jump in signal with a change in slope. This would appear as a "kink" in the magnetization data above as the majority of the spins align themselves with the external field. An antiferromagnetic order would be represented by a sudden downturn in magnetization [[12]]. This lack of magnetization down to low T is characteristic of a QSL. The units on the y-axis is in Bohr magneton per fundamental Unit (**F.U**), this is akin to per molecule made out of the stoichiometric ratio for the material. The external field strength was around 0.1 Tesla.

Figure 22: Magnetic order examples [[12]]

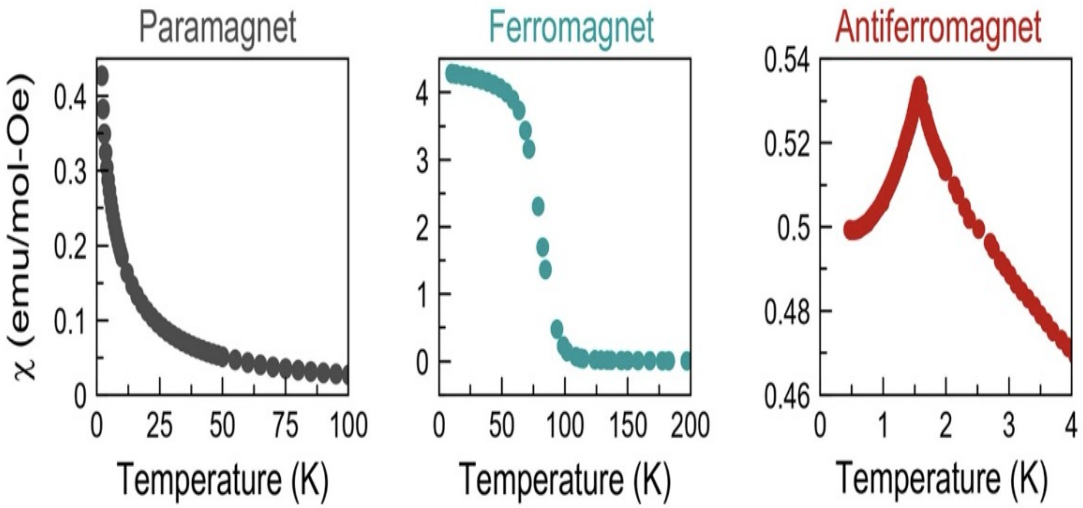

[[12]] Taking a look at some examples of what paramagnetic order would appear as in magnetization vs temperature. The ferromagnetic order is seen as a transition upwards in magnetic susceptibility, the antiferromagnetic order as a "cusp" downwards.

Figure 23: Curie–Weiss Fitting$_c$

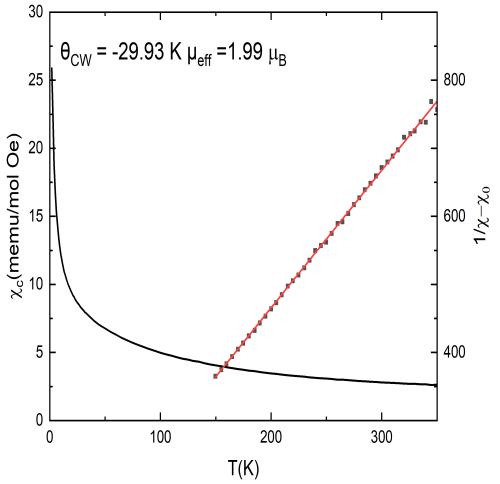

Figure 24: Curie–Weiss Fitting$_{ab}$

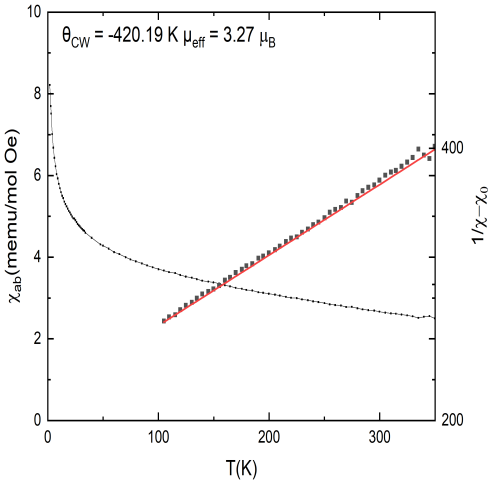

I will now go over the detail in the magnetic data above. On the left y-axis is the magnetic susceptibility, where the magnetization has been corrected for the applied external magnetic field. This is then further normalized for per mole of substance using the mass and molar mass of the material. The right y-axis is a fitting that is achieved using the following steps. First we only take the high temperature data around 100 K to 300 K for magnetic susceptibility. Plot this :

$$\chi^{-1} vs \;\; T$$

Now using the Curie-Weiss function above in the methods section:

$$\chi^{-1} = \frac{T - \theta_{CW}}{C}$$

If we use a linear fitting: the slope is 1/C, the intercept is $\frac{\theta_{CW}}{C}$. This fitting is

represented in red on the right, whereas the $1/\chi$ data is a scatter plot on the same scale on the right y-axis. Due to paramagnetic contributions that are independent of of temperature, such as Pauli Paramagnetic and Van Vleck paramagnetic, the simplified equation above is changed to:

$$\chi = \frac{C}{T - \theta_{CW}} + \chi_0$$

$$\chi^{-1} = \frac{T - \theta_{CW}}{\chi_0(T - \theta_{CW}) + C}$$

where the constant χ_0 represents this independent paramagnetic contribution. The negative Curie-Weiss temperature of 29.3 K indicates a antiferromagnetic coupling. This antiferromagnetic coupling is further seen with the fitting in the ab-direction that boasts a large negative -420 K Curie-Weiss temperature. The effective moment in the ab-direction is also higher when compared to c-direction per ion which tracks with the higher signal in the ab-direction.

The data in these sections provides credence for the existence of a heavy-fermion insulator that also seems to be an frustrated QSL. The last set of data takes a look at the hall effect data for ($Ba_4Nb_{1.163}Ru_{2.837}O_{12}$). This material is very similar to the material studied above as a heavy-fermion insulator without any long range order. The unique data present in the Hall effect data will be discussed as it raises important questions prompting further research.

4.4 Hall effect for $Ba_4Nb_{1.163}Ru_{2.837}O_{12}$

Figure 25: $Resistivity_{Ba_4Nb_{1.163}Ru_{2.837}O_{12}}$ [[1]]

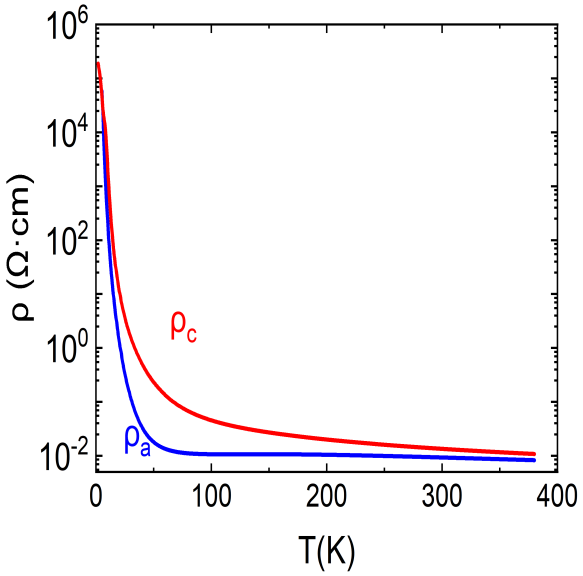

Figure 26: $Magnetization_{Ba_4Nb_{1.163}Ru_{2.837}O_{12}}$ [[1]]

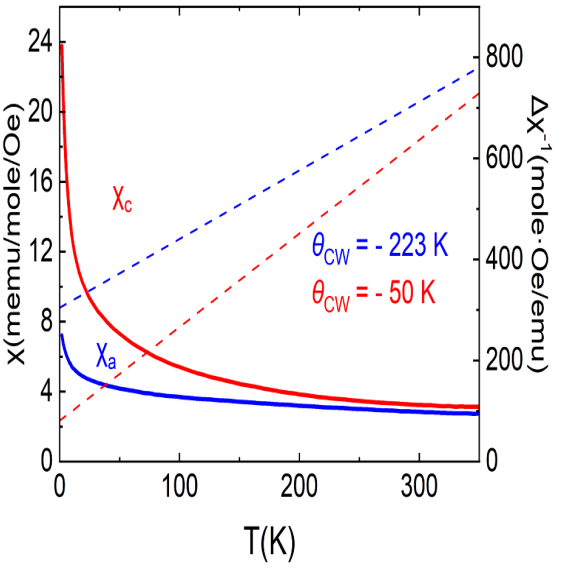

The data above was collected by graduate students in the group rather than me. We see here that this doping level of Nb has similar properties to the sample studied above [[1]]. With it being an insulator and a large negative θ_{CW} temperature indicating antiferromagnetic coupling. Also important to note here, in the resistivity data while there are differences in magnitude between the two directions, the general trend is about the same. This makes the differences in hall data especially interesting.

Figure 27: Hall effect

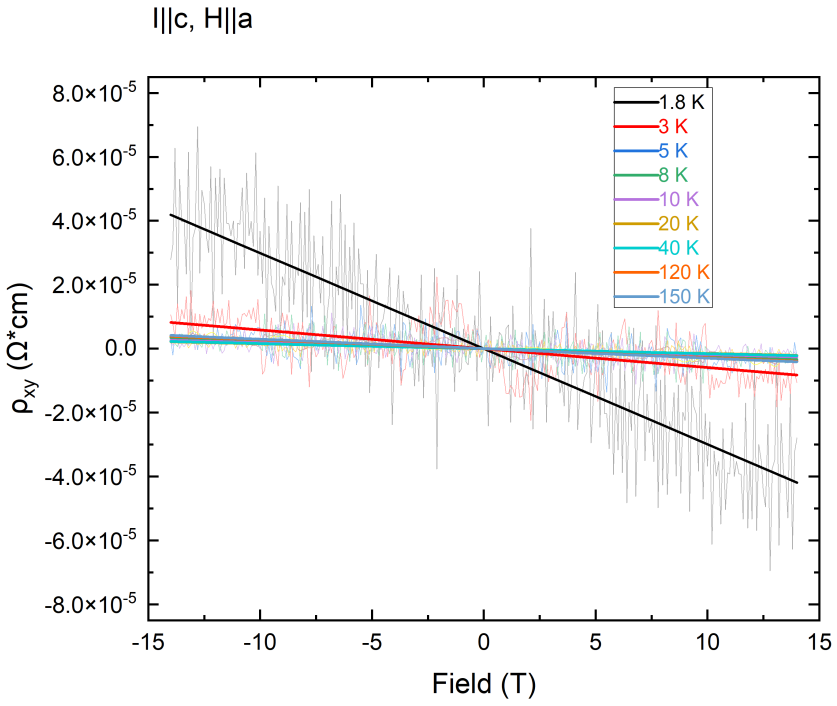

In the Figure above ρ_{xy} represents the transverse resistivity. The noise in the faded data is due to the high resistivity and the relatively small size of the sample increasing the noise to signal ratio. The solid lines are a linear trend that's been fitted to the data. The hall resistivity is measured as a function of field at specific temperatures. To see why the resistivity gets more flat as you increase temperature:

$$V_H = -\frac{-IB}{nqd}$$

Where I is the applied current, B is the external magnetic field, n is the charge carrier density, q is the charge of the charge carrier, and d is the thickness of the material. As the temperature increases the dominating factor is the charge carrier density that

increases in insulators, hence the resistivity for the hall effect falls along with the hall voltage.

We can then calculate the charge carrier density as

$$V_H = -\frac{-IB}{nqd}$$

$$V_H = -\frac{-R_H IB}{d}$$

Where R_H is the hall coefficient and is equal to the slope of the linear fittings above:

$$R_H = \frac{1}{nq}$$

Plotting n:

Figure 28: Charge carrier density

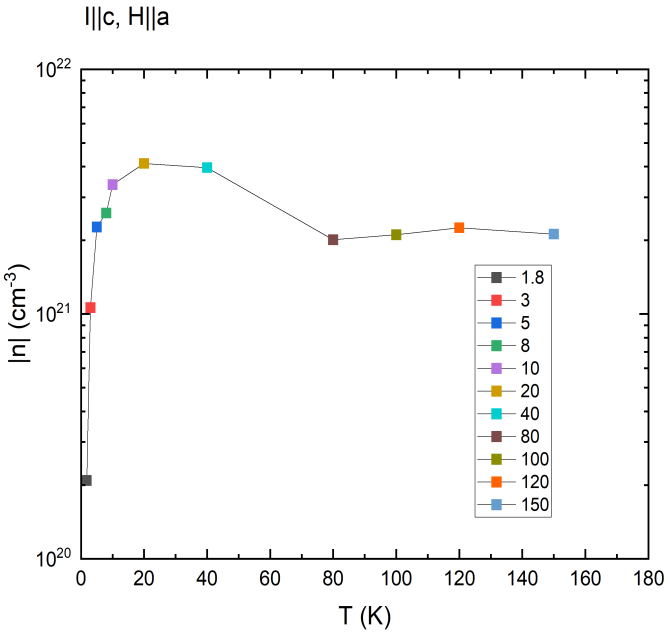

The plot represents the absolute value of n vs temperature. We see a strange trend in the charge carrier density, as it rises and seems to peak around 20 K and then falls before leveling off. This is unexpected as we should see a general rise in charge carrier density as temperature increases. This is because the thermal entropy allows the electrons to move to the conduction band and reduces scattering caused by impurities in the material. What is especially interesting is if we plot the charge carrier density when measuring hall in the ab-direction we see a typical insulator's behavior:

Figure 29: Charge carrier density

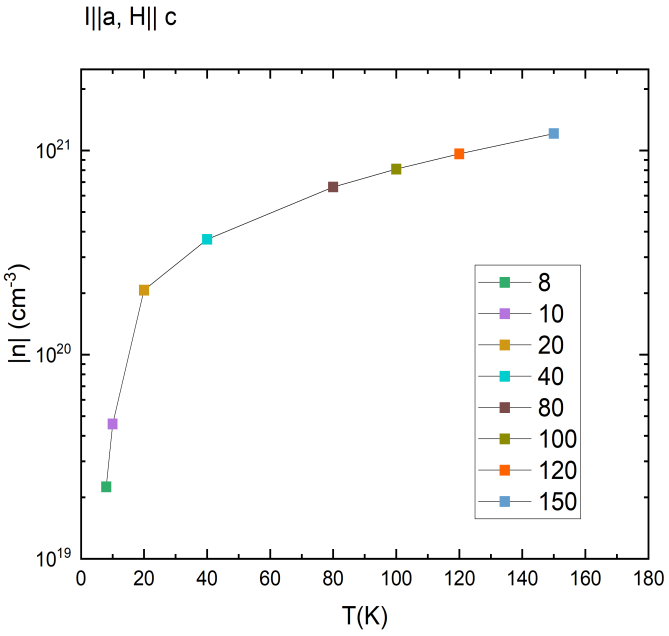

It is important to note that due to the extremely high resistance, the lower temperature values for hall effect were not able to be calculated. Still, this indicates an anisotropy within the material, making this behavior in the charge carrier density for the hall effect especially motivating and raises another question prodding further research.

5 Summary

This material is a host to a variety of exotic quantum states. In this thesis, the insulating Nb rich side of the material has been studied using a variety of physical property measurements such as heat capacity, resistivity, hall effect, and magnetization. Through the magnetization data, we can see the lack of long range magnetic order indicating the existence of a QSL. The heat capacity data shows a sharp linear relationship of HC vs temperature confirming the heavy-fermion nature of this material. Lastly the strange data in the hall effect results of the material showed an anisotropy indicated by a anomalous decline in charge carrier density in only one direction.

6 Future research

There are many avenues to continue work on this material in the future. Seeing if this anisotropic behavior is seen in all of the Nb doping regions including the conducting metallic states. To better confirm the lack of a magnetic order, going to milli-Kelvin regions and conducing ac susceptibility or SQUID measurements would further prove the existence of a QSL.

References

[1] Hengdi Zhao et al. *Heavy-fermion strange metal and quantum spin liquid in a 4d-electron trimer lattice*. arXiv:2305.01033 [cond-mat]. May 2023. URL: http://arxiv.org/abs/2305.01033 (visited on 03/12/2024).

[2] S. Burdin, D. R. Grempel, and A. Georges. "Heavy-fermion and spin-liquid behavior in a Kondo lattice with magnetic frustration". In: *Physical Review B* 66.4 (July 2002). Publisher: American Physical Society, p. 045111. DOI: 10.1103/PhysRevB.66.045111. URL: https://link.aps.org/doi/10.1103/PhysRevB.66.045111 (visited on 03/12/2024).

[3] Piers Coleman. *Heavy Fermions and the Kondo Lattice: a 21st Century Perspective*. arXiv:1509.05769 [cond-mat]. Sept. 2015. URL: http://arxiv.org/abs/1509.05769 (visited on 03/12/2024).

[4] Marcelo Jaime et al. "Closing the spin gap in the Kondo insulator Ce3Bi4Pt3 at high magnetic fields". en. In: *Nature* 405.6783 (May 2000). Publisher: Nature Publishing Group, pp. 160–163. ISSN: 1476-4687. DOI: 10.1038/35012027. URL: https://www.nature.com/articles/35012027 (visited on 03/12/2024).

[5] S. Kondo et al. "LiV 2 O 4 : A Heavy Fermion Transition Metal Oxide". en. In: *Physical Review Letters* 78.19 (May 1997), pp. 3729–3732. ISSN: 0031-9007, 1079-7114. DOI: 10.1103/PhysRevLett.78.3729. URL: https://link.aps.org/doi/10.1103/PhysRevLett.78.3729 (visited on 03/14/2024).

[6] Chao Yang et al. "A strange metal in a bosonic system". In: *Nature* 601.7892 (Jan. 2022). arXiv:2105.02654 [cond-mat], pp. 205–210. ISSN: 0028-0836, 1476-

4687. DOI: 10.1038/s41586-021-04239-y. URL: http://arxiv.org/abs/2105.02654 (visited on 03/12/2024).

[7] Lucile Savary and Leon Balents. "Quantum spin liquids: a review". en. In: *Reports on Progress in Physics* 80.1 (Jan. 2017), p. 016502. ISSN: 0034-4885, 1361-6633. DOI: 10.1088/0034-4885/80/1/016502. URL: https://iopscience.iop.org/article/10.1088/0034-4885/80/1/016502 (visited on 03/12/2024).

[8] Jinsheng Wen et al. "Experimental identification of quantum spin liquids". en. In: *npj Quantum Materials* 4.1 (Apr. 2019). Publisher: Nature Publishing Group, pp. 1–9. ISSN: 2397-4648. DOI: 10.1038/s41535-019-0151-6. URL: https://www.nature.com/articles/s41535-019-0151-6 (visited on 03/14/2024).

[9] Quantum Design. *Electrical Transport Option (ETO) User's Manual*. Tech. rep.

[10] P. Debye. "Zur Theorie der spezifischen Wärmen". en. In: *Annalen der Physik* 344.14 (1912). _eprint: https://onlinelibrary.wiley.com/doi/pdf/10.1002/andp.19123441404, pp. 789–839. ISSN: 1521-3889. DOI: 10.1002/andp.19123441404. URL: https://onlinelibrary.wiley.com/doi/abs/10.1002/andp.19123441404 (visited on 03/11/2024).

[11] Quantum Design. *Heat Capacity Option User's Manual*. Tech. rep.

[12] Sam Mugiraneza and Alannah M. Hallas. "Tutorial: a beginner's guide to interpreting magnetic susceptibility data with the Curie-Weiss law". en. In: *Communications Physics* 5.1 (Apr. 2022). Publisher: Nature Publishing Group, pp. 1–12. ISSN: 2399-3650. DOI: 10.1038/s42005-022-00853-y. URL: https://www.nature.com/articles/s42005-022-00853-y (visited on 03/11/2024).

[13] Jonny McAneney. “Characteristics of Thin and Ultrathin Ferroelectric Capacitor Structures”. PhD thesis. Sept. 2005.